

Supplementary Data

**Mononuclear, Helical Binuclear Palladium and Lithium Complexes Bearing a
New Pyrrole-based NNN-Pincer Ligand: Fluxional Property**
Debasish Ghorai, Shanish Kumar and Ganesan Mani*

Department of Chemistry, Indian Institute of Technology, Kharagpur, India 721 302

Fax: +91 3222 282252, E-mail: gmani@chem.iitkgp.ernet.in

Table of contents

<i>I.</i>	<i>NMR and IR spectra</i>	<i>S2</i>
<i>II.</i>	<i>X-ray Crystallography</i>	<i>S16</i>

I. NMR and IR spectra

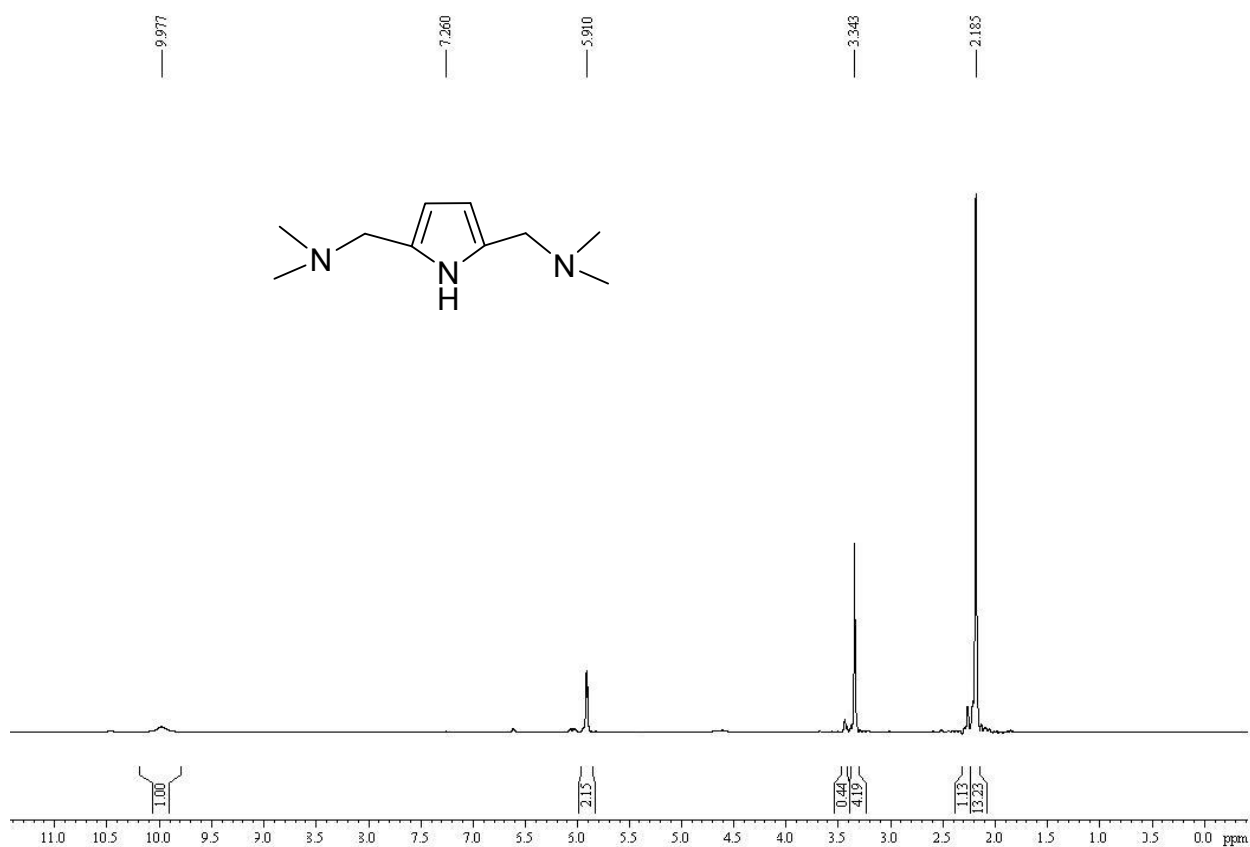


Figure S1. ¹H NMR spectrum of 2,5-bis(dimethylaminomethyl)pyrrole, **1** in CDCl₃.

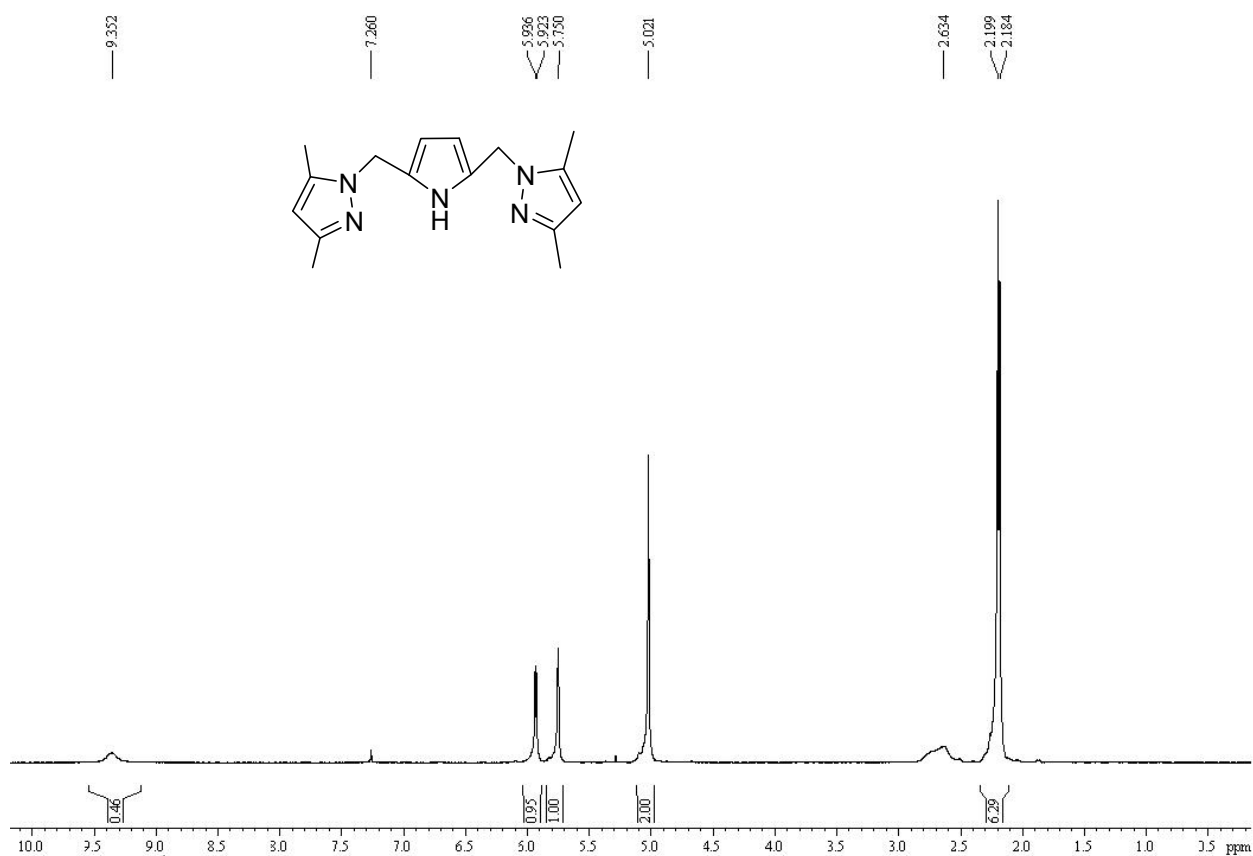


Figure S2. ¹H NMR spectrum of 2,5-bis(3,5-dimethylpyrazolylmethyl)pyrrole **2** in CDCl₃.

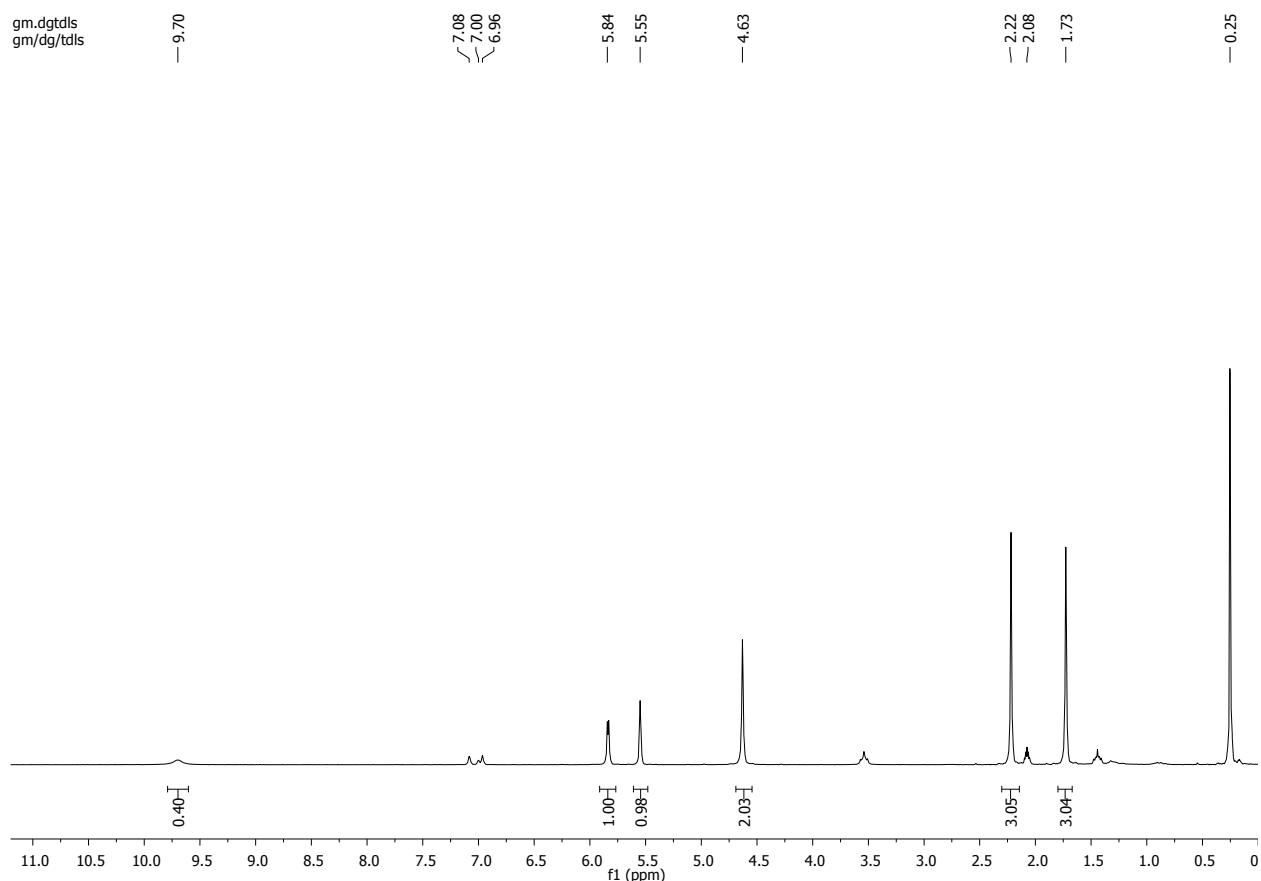


Figure S3. ^1H NMR spectrum of 2,5-bis(3,5-dimethylpyrazolylmethyl)pyrrole **2** in toluene- d_8 .

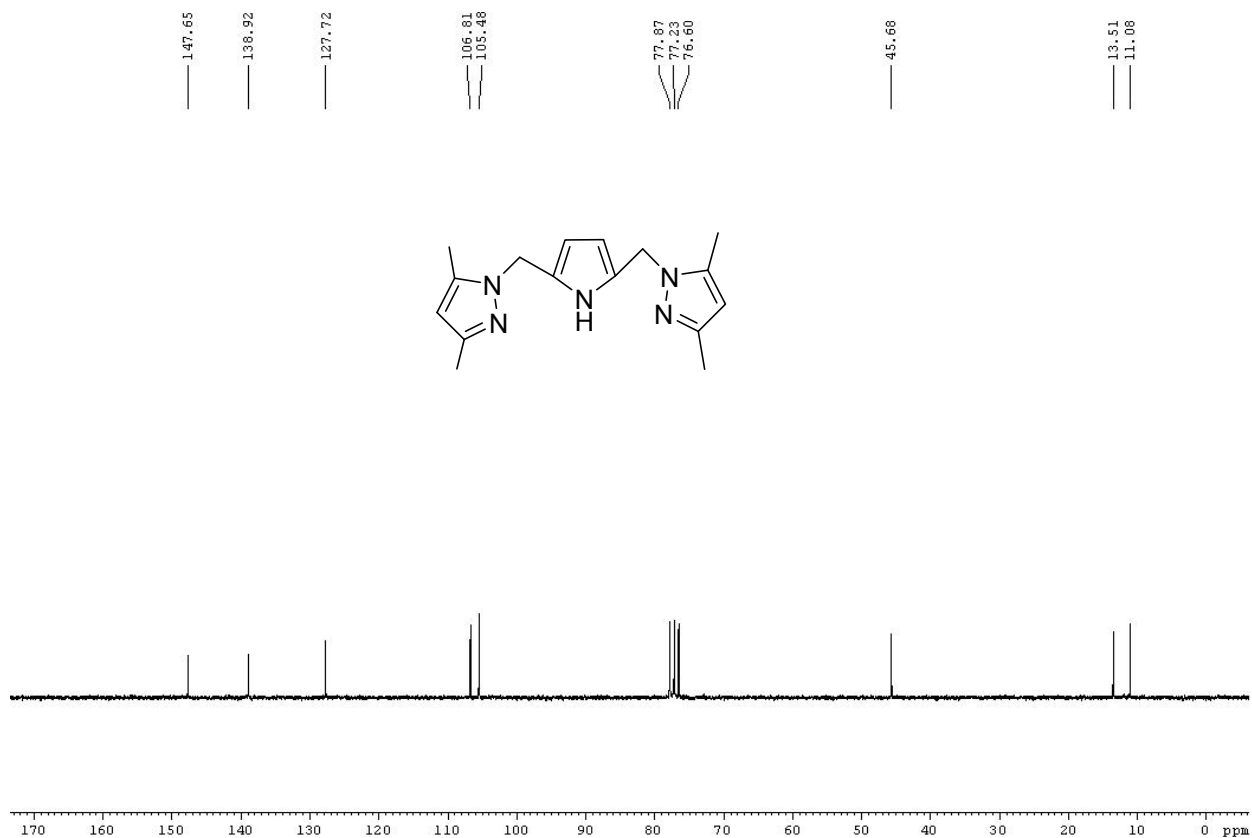


Figure S4. $^{13}\text{C}\{^1\text{H}\}$ NMR spectrum of 2,5-bis(3,5-dimethylpyrazolylmethyl)pyrrole **2** in CDCl_3 .

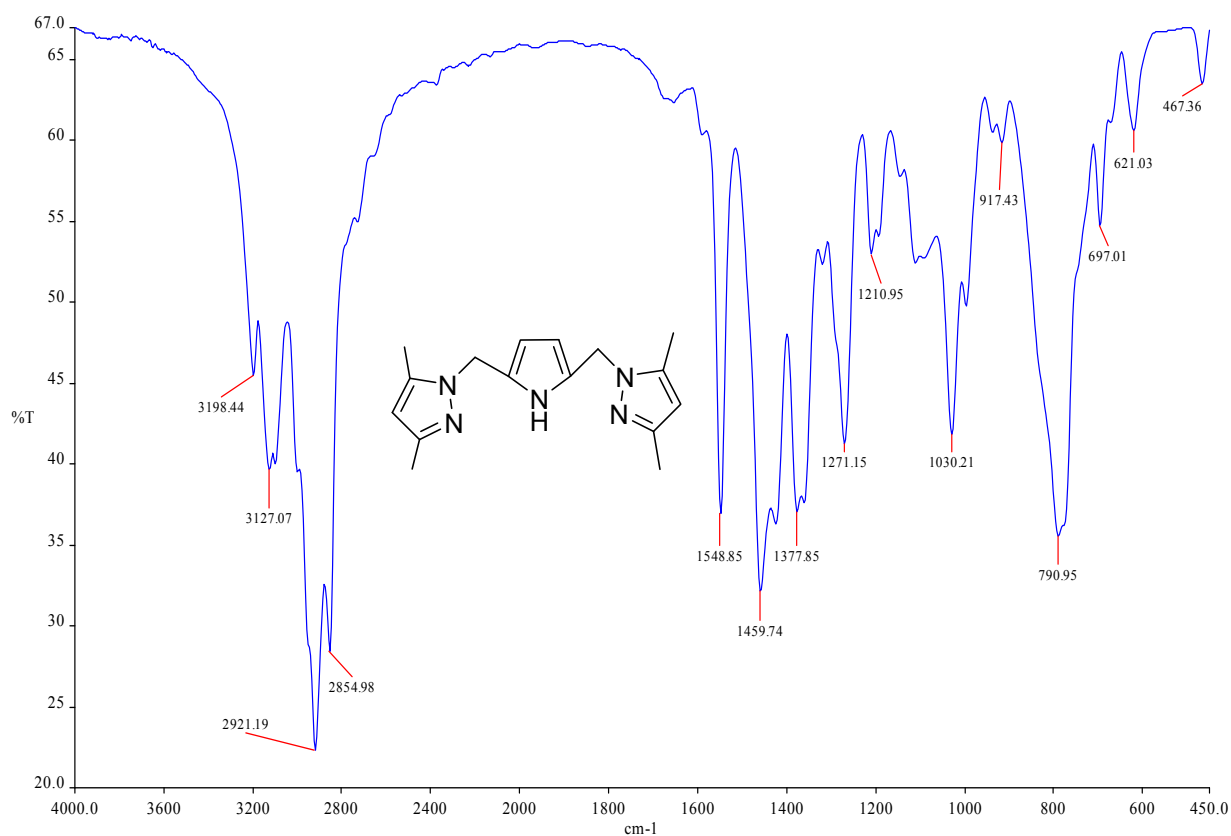


Figure S5. IR spectrum of 2,5-bis(3,5-dimethylpyrazolylmethyl)pyrrole **2** recorded as a KBr disc.

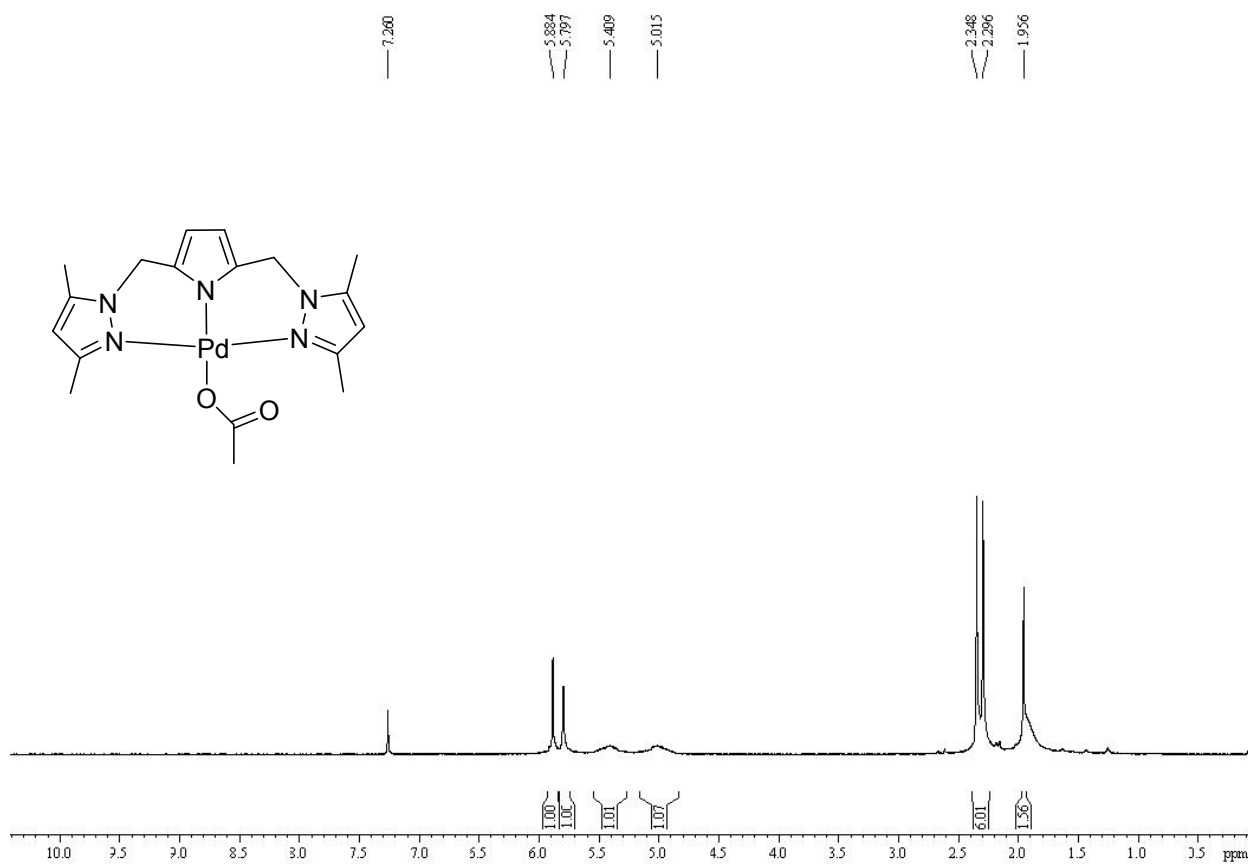


Figure S6. ^1H NMR spectrum of $[\text{Pd}(\text{OAc})\{\text{C}_4\text{H}_2\text{N}-2,5-(\text{CH}_2\text{Me}_2\text{pz})_2-\text{N},\text{N},\text{N}\}]$, **3** in CDCl_3 .

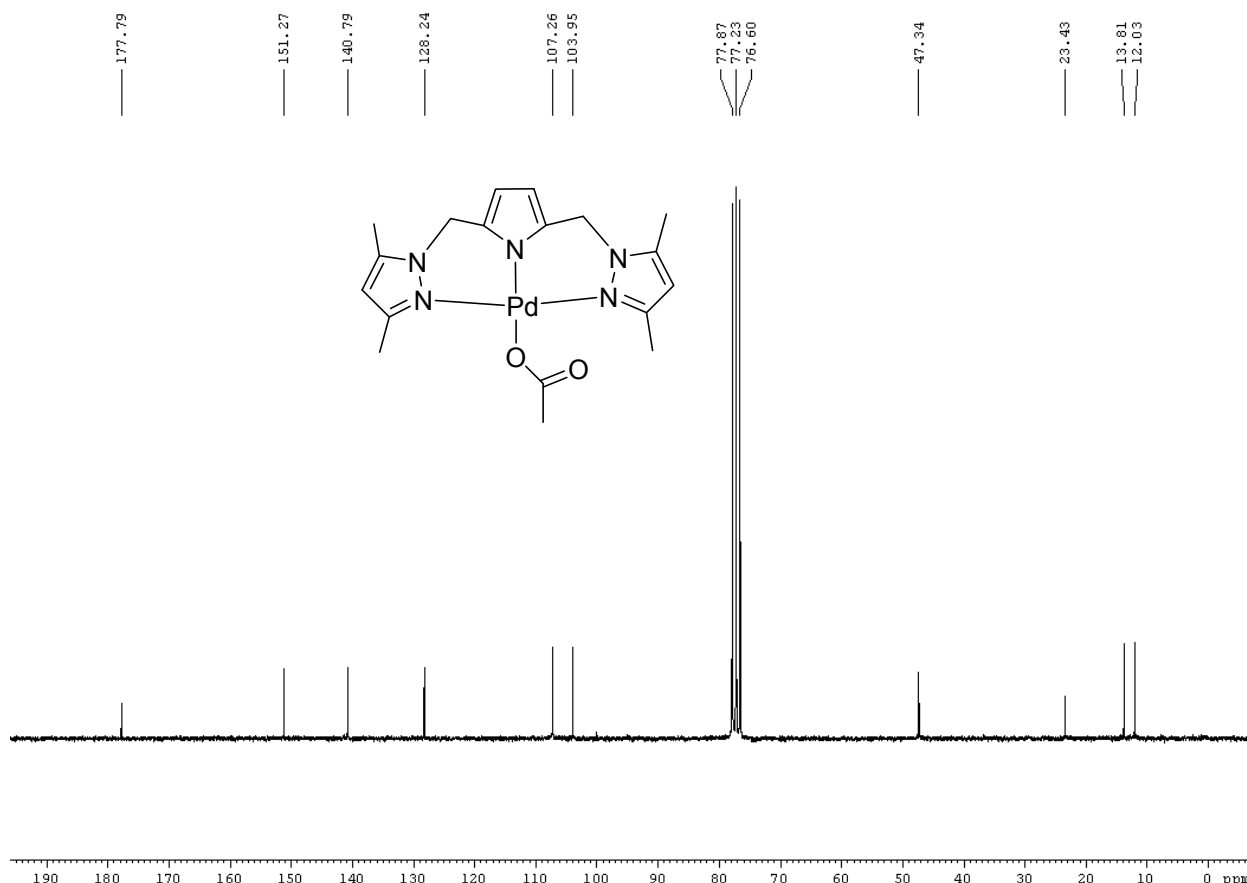


Figure S7. $^{13}\text{C}\{^1\text{H}\}$ NMR spectrum of $[\text{Pd}(\text{OAc})\{\text{C}_4\text{H}_2\text{N}-2,5-(\text{CH}_2\text{Me}_2\text{pz})_2-\text{N},\text{N},\text{N}\}]$, **3** in CDCl_3 .

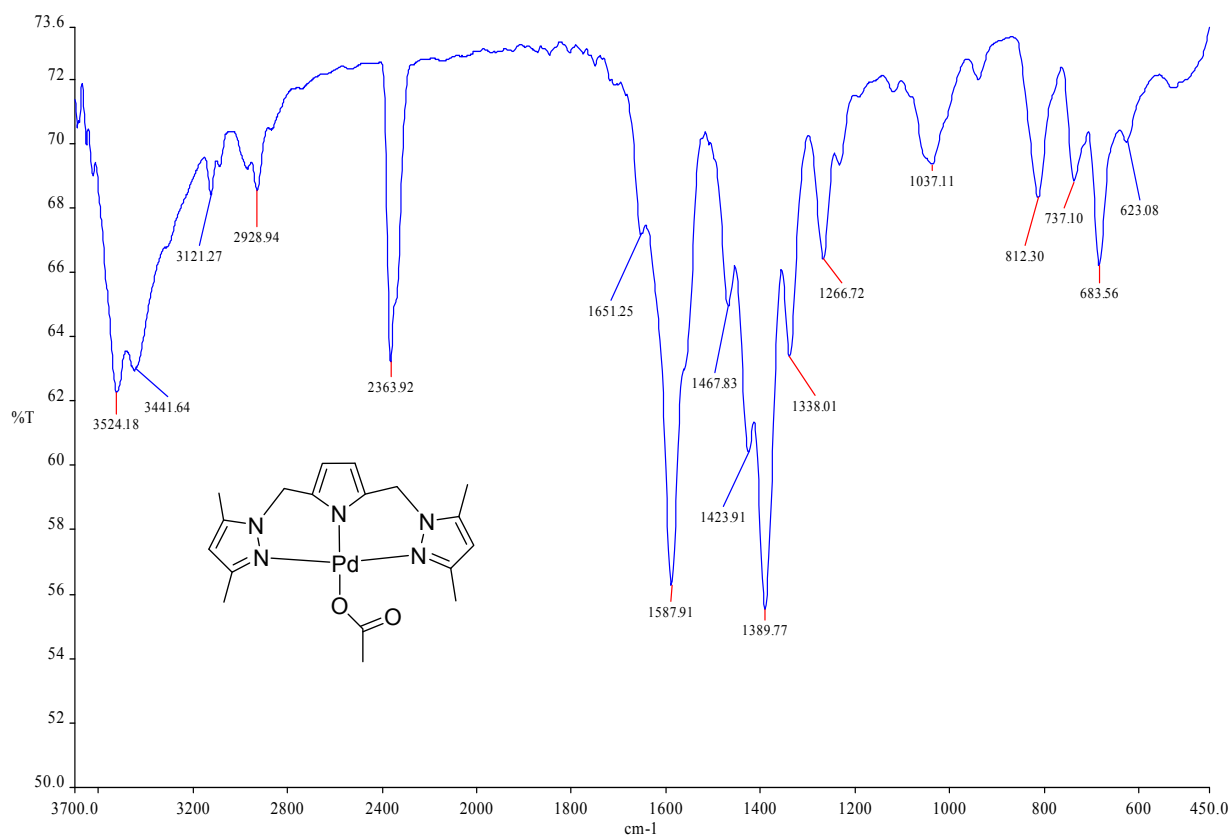


Figure S8. IR spectrum of $[\text{Pd}(\text{OAc})\{\text{C}_4\text{H}_2\text{N}-2,5-(\text{CH}_2\text{Me}_2\text{pz})_2-\text{N},\text{N},\text{N}\}]$, **3** recorded as a KBr disc.

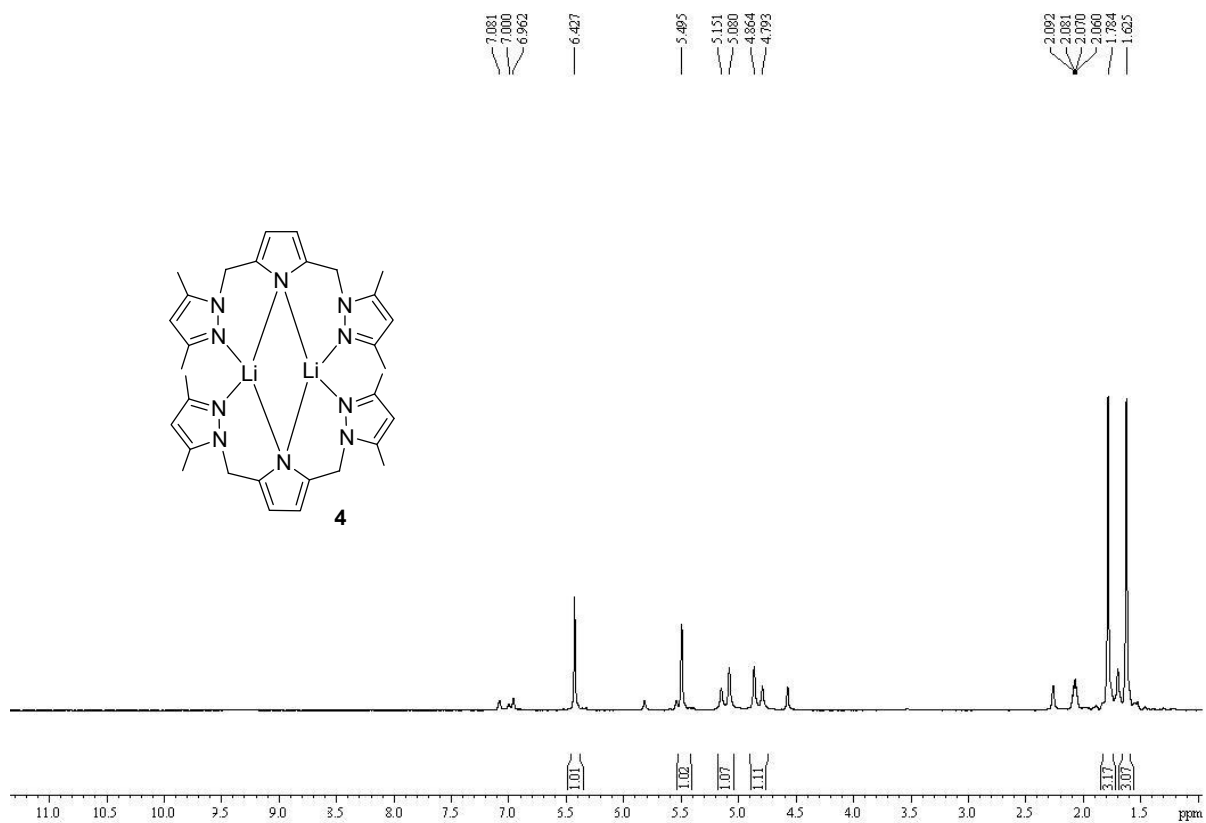


Figure S9. ^1H NMR spectrum of $[\text{Li}\{\mu\text{-C}_4\text{H}_2\text{N-2,5-(CH}_2\text{Me}_2\text{pz)}_2\text{-N,N,N}\}]_2$, **4** in toluene- d_8 .

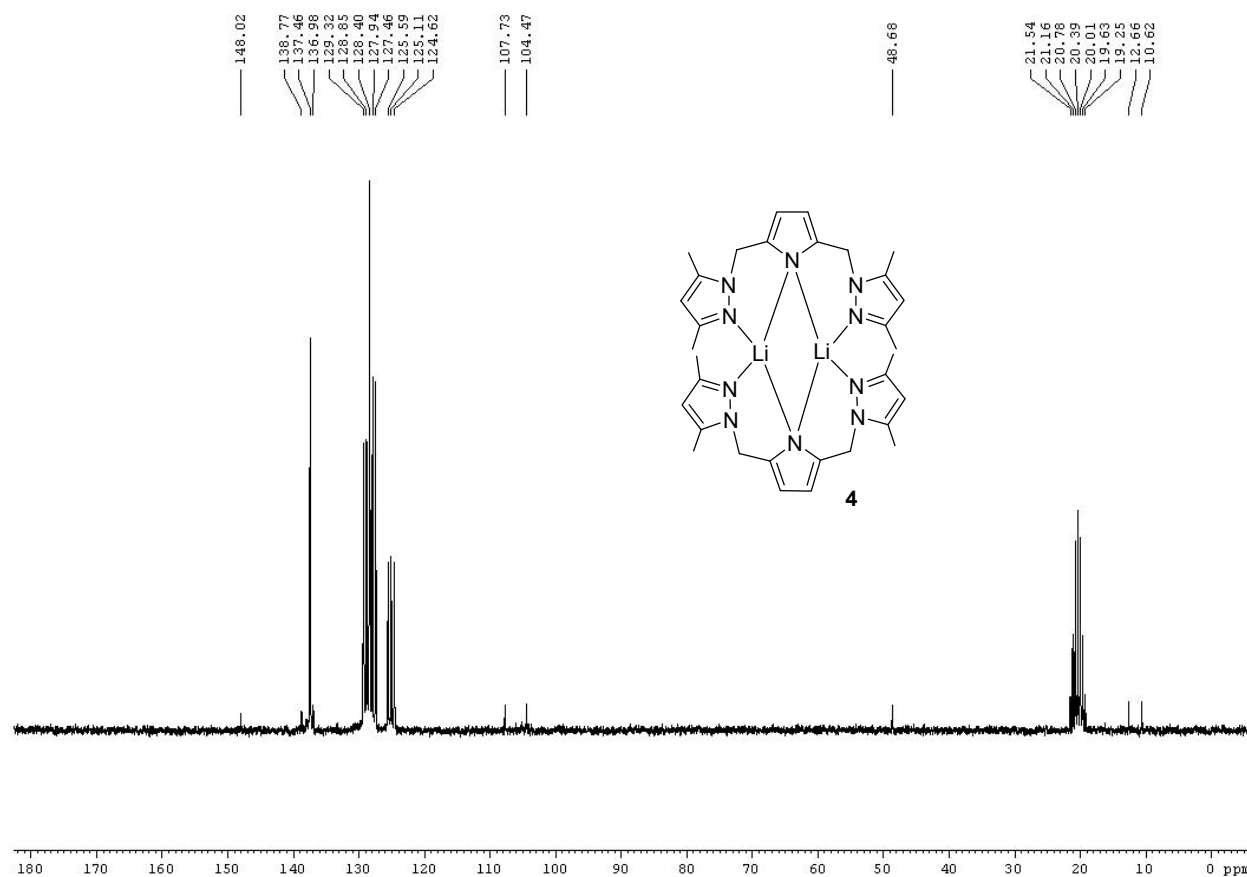


Figure S10. $^{13}\text{C}\{^1\text{H}\}$ NMR spectrum of $[\text{Li}\{\mu\text{-C}_4\text{H}_2\text{N-2,5-(CH}_2\text{Me}_2\text{pz)}_2\text{-N,N,N}\}]_2$, **4** in toluene- d_8 .

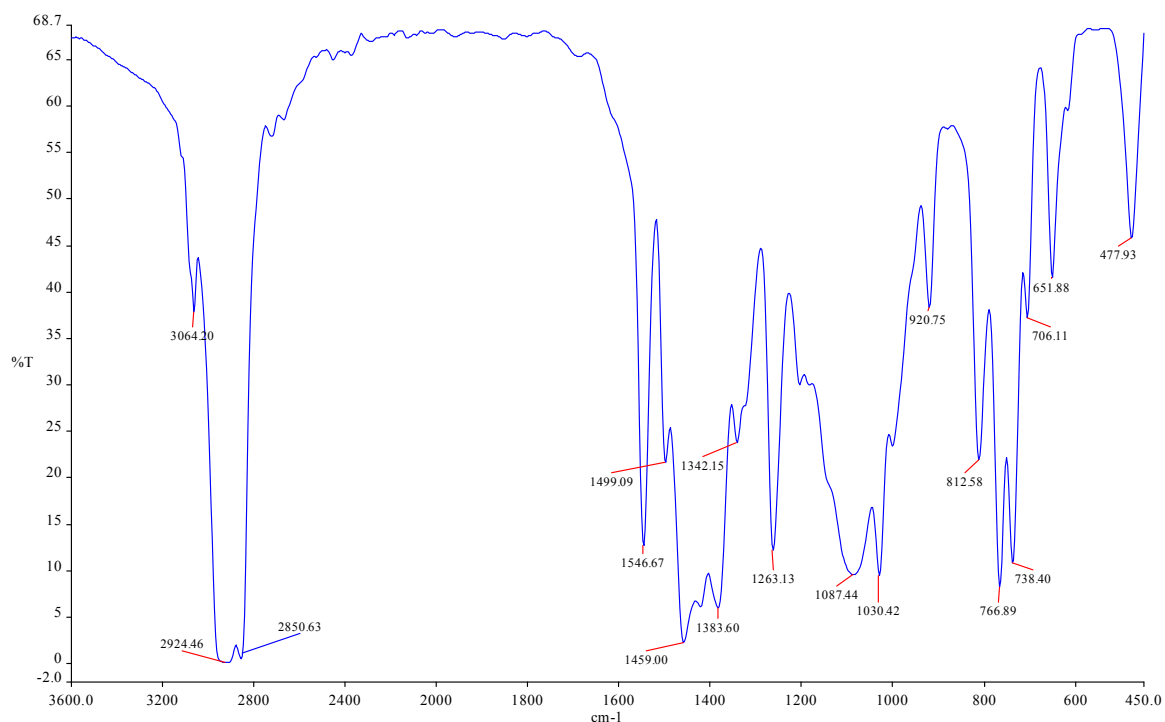


Figure S11. IR spectrum of $[\text{Li}\{\mu\text{-C}_4\text{H}_2\text{N-2,5-(CH}_2\text{Me}_2\text{pz)}_2\text{-N,N,N}\}]_2$, **4** recorded as a Nujol mull.

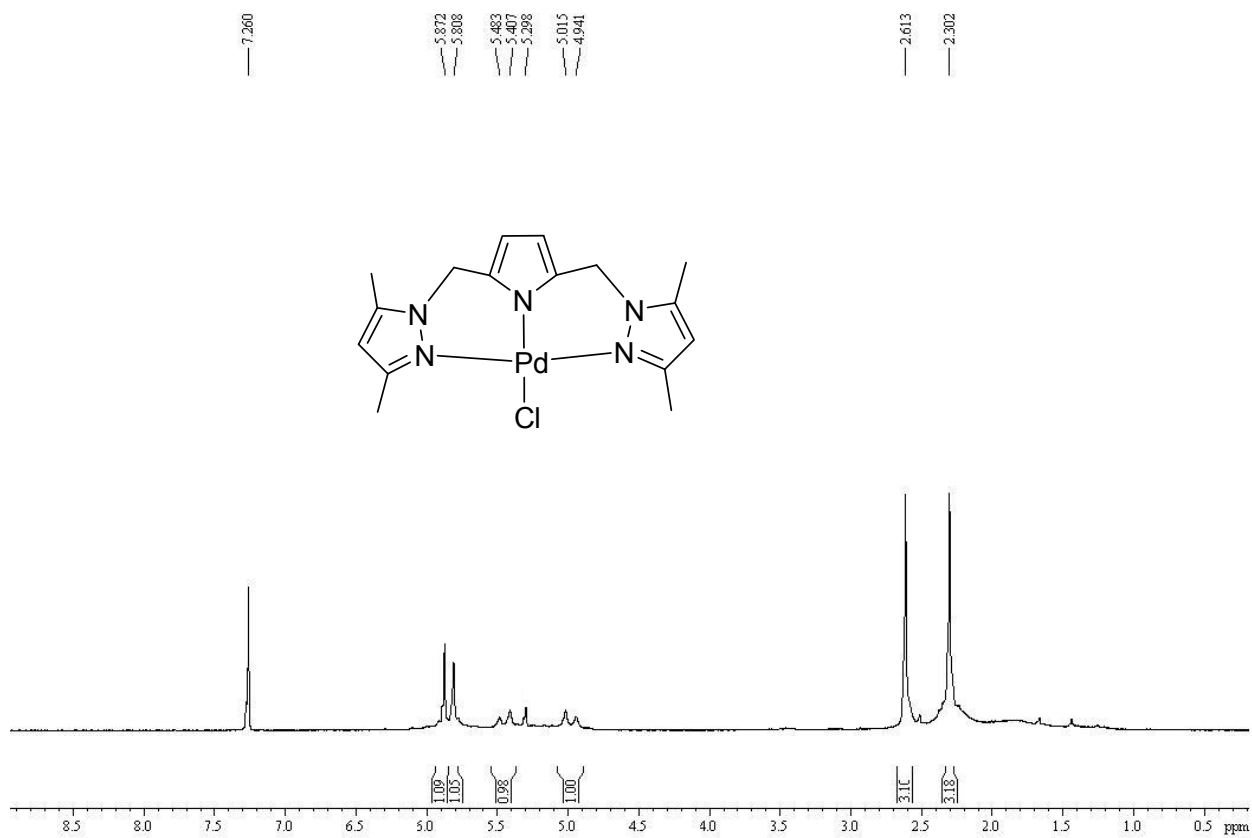


Figure S12. ^1H NMR spectrum of $[\text{PdCl}\{\text{C}_4\text{H}_2\text{N-2,5-(CH}_2\text{Me}_2\text{pz)}_2\text{-N,N,N}\}]$ **5** in CDCl_3 .

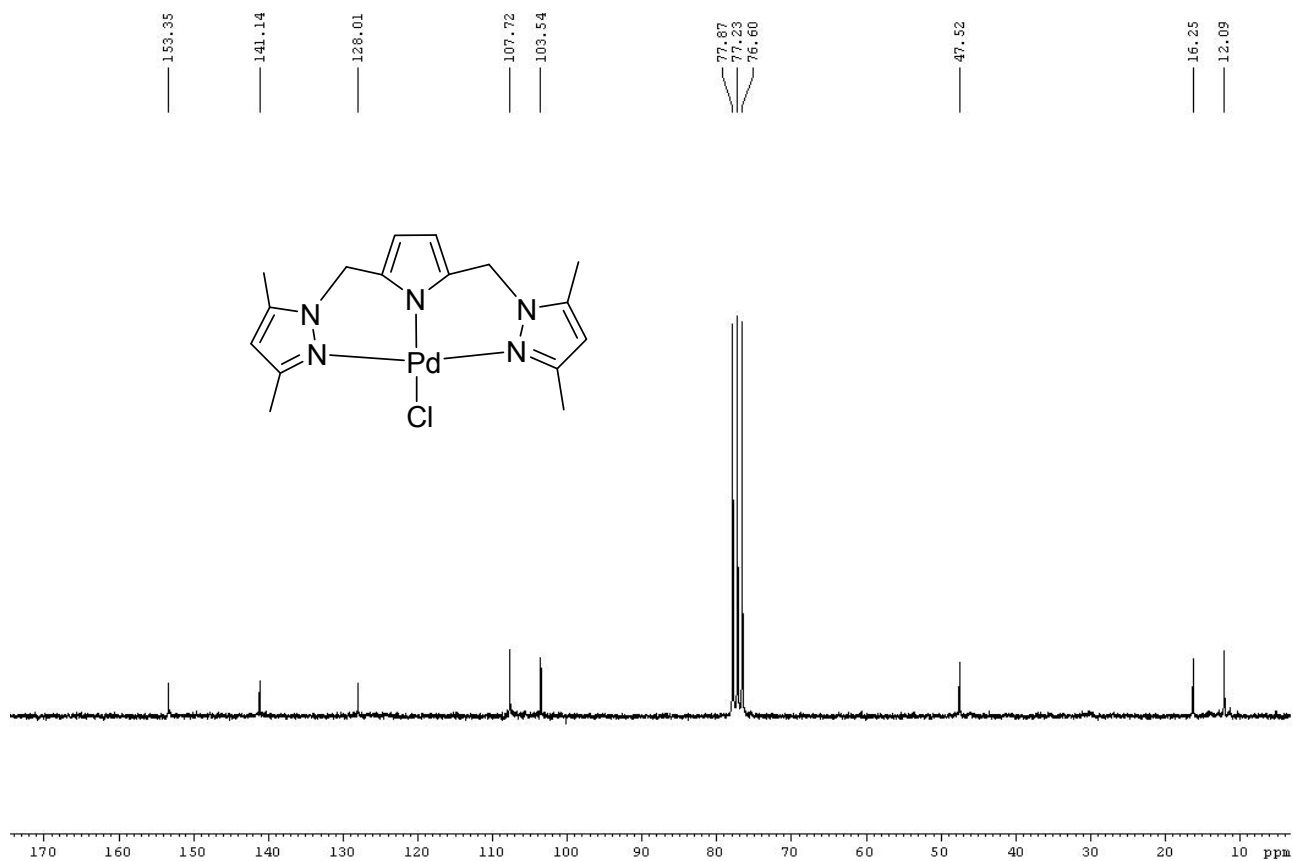


Figure S13. $^{13}\text{C}\{^1\text{H}\}$ NMR spectrum of $[\text{PdCl}\{\text{C}_4\text{H}_2\text{N}-2,5-(\text{CH}_2\text{Me}_2\text{pz})_2\text{-}N,N,N\}]$ **5** in CDCl_3 .

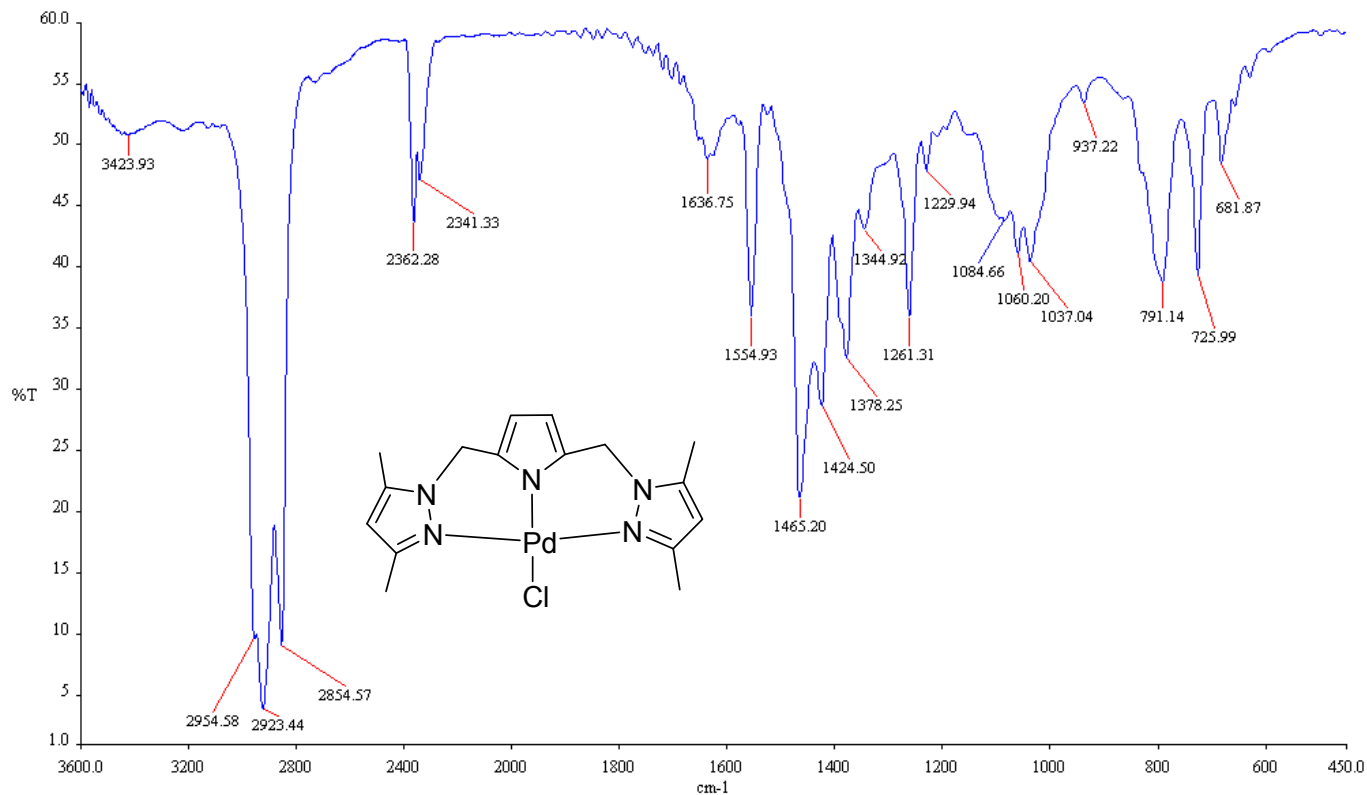


Figure S14. IR spectrum of $[\text{PdCl}\{\text{C}_4\text{H}_2\text{N}-2,5-(\text{CH}_2\text{Me}_2\text{pz})_2\text{-}N,N,N\}]$ **5** recorded as a Nujol mull.

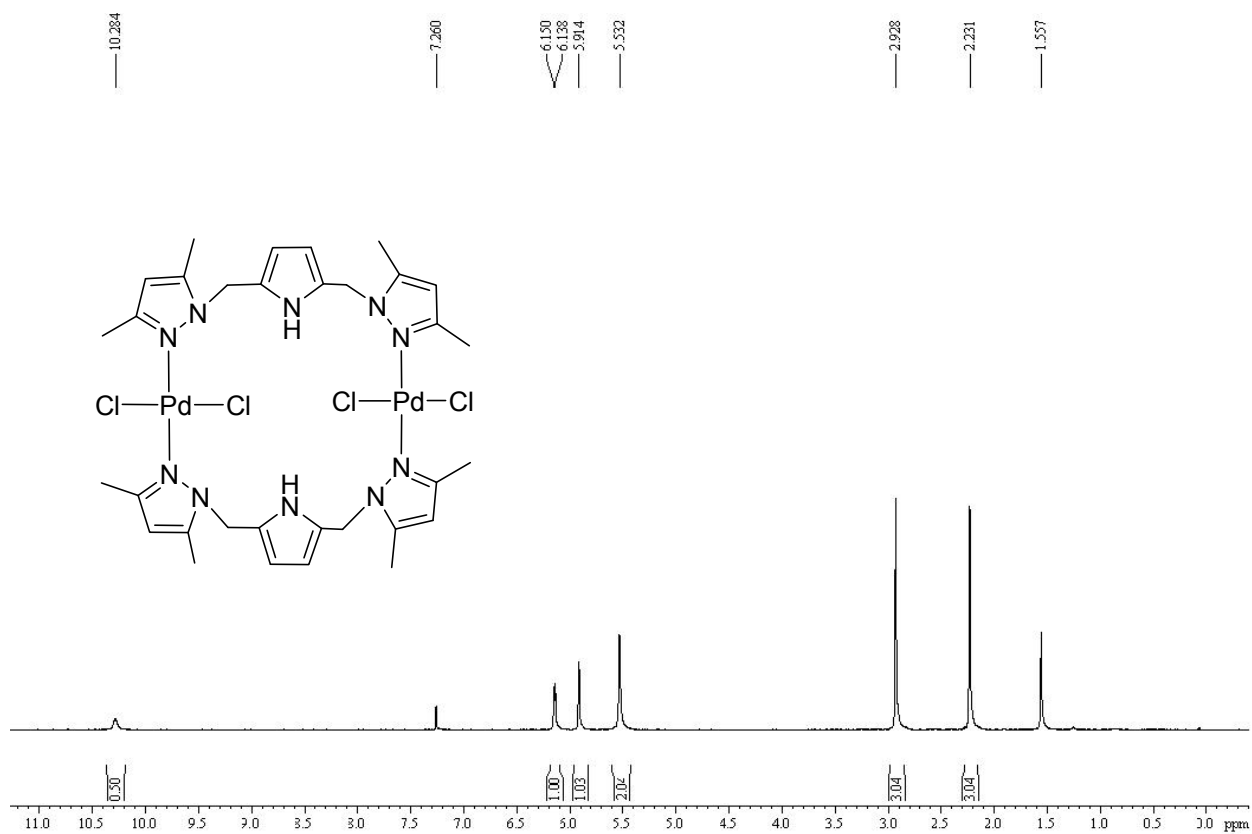


Figure S15. ¹H NMR spectrum of [Pd₂Cl₄{μ-C₄H₃N-2,5-(CH₂Me₂pz)₂-N,N}₂] **6** in CDCl₃.

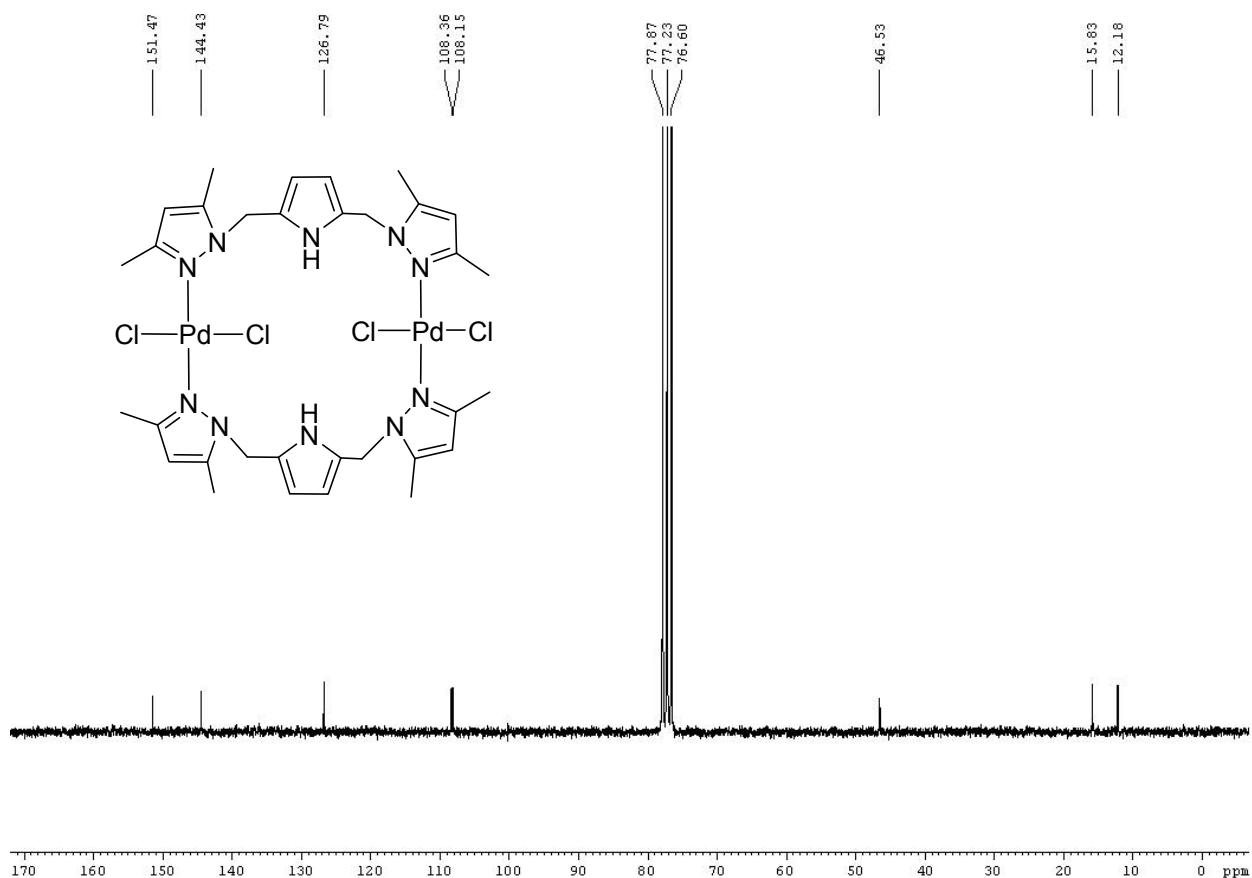


Figure S16. ¹³C{¹H} NMR spectrum [Pd₂Cl₄{μ-C₄H₃N-2,5-(CH₂Me₂pz)₂-N,N}₂] **6** in CDCl₃.

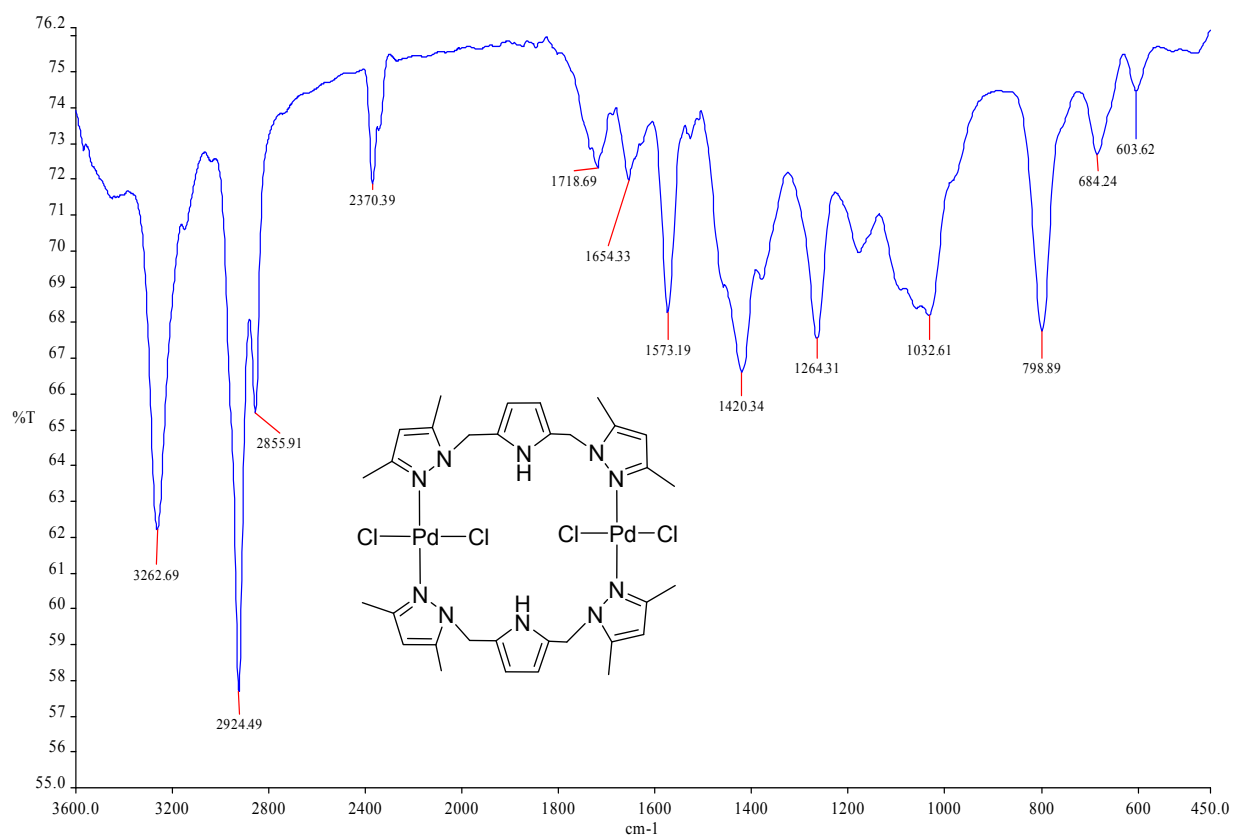


Figure S17. IR spectrum of $[\text{Pd}_2\text{Cl}_4\{\mu\text{-C}_4\text{H}_3\text{N-2,5-(CH}_2\text{Me}_2\text{pz)}_2\text{-N,N}\}_2]$ **6** recorded as a KBr disc.

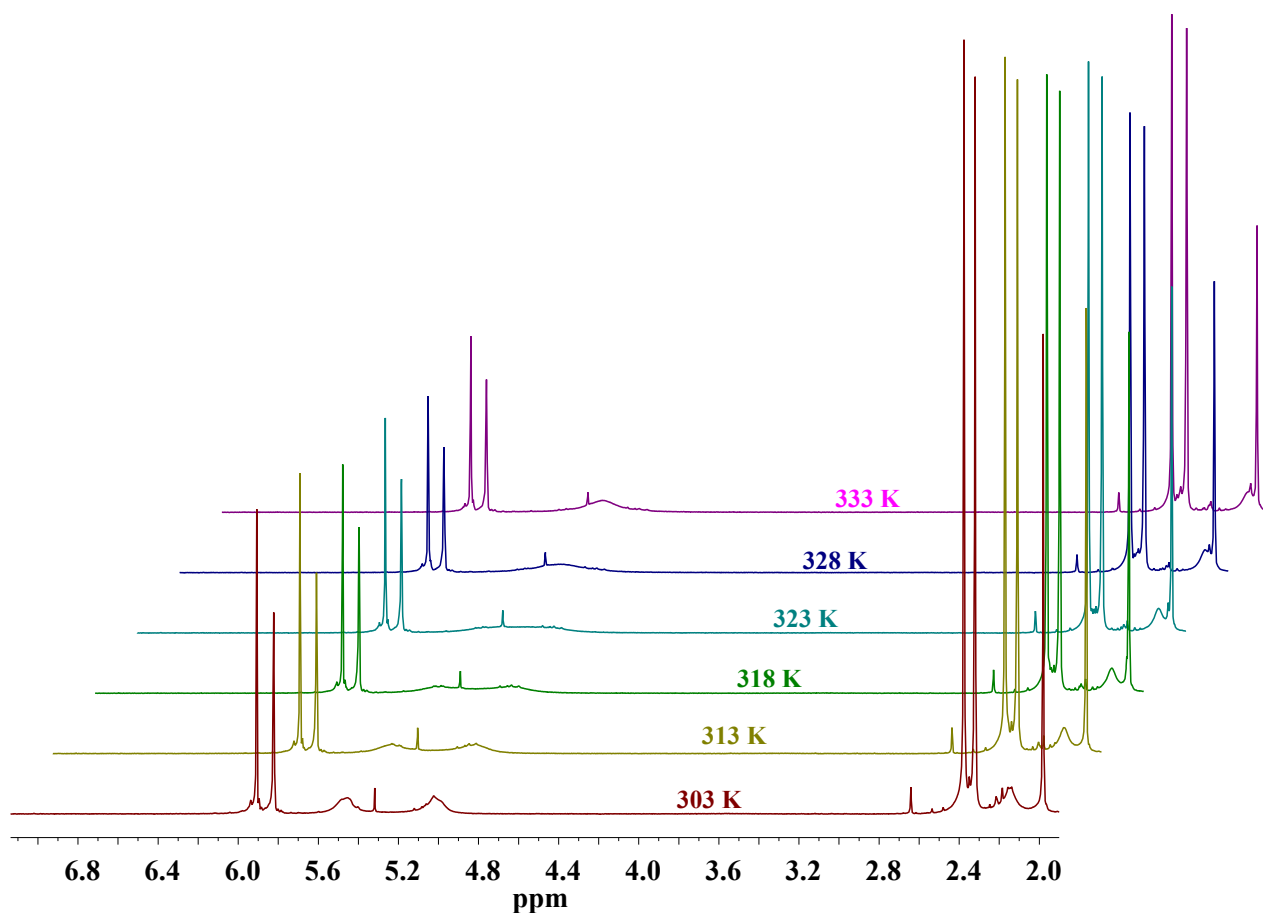


Figure S18. Variable-temperature ¹H NMR spectra (400 MHz) of complex **3** in CDCl₃ (0.04 M) showing a broad singlet for its diastereotopic methylene protons at 50 °C due to the fast interconversion between the two enantiomers on the NMR time scale. The coalescence temperature *T_c* is the same as that observed for 0.02 M sample.

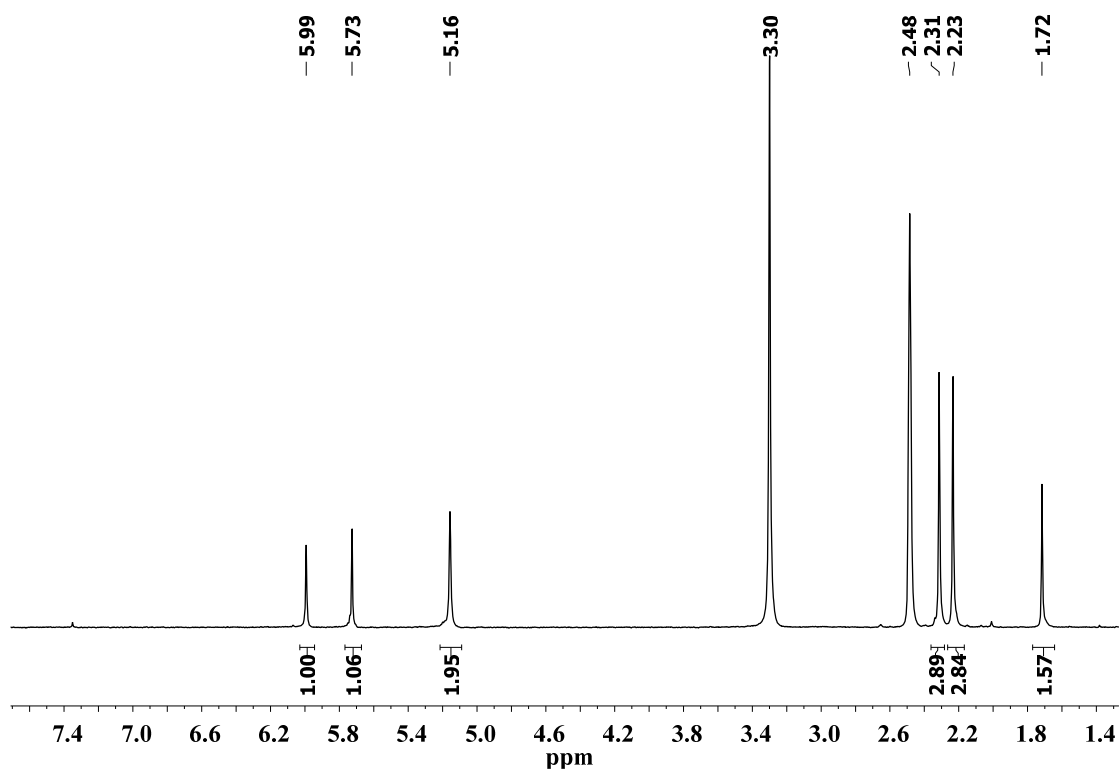


Figure S19. ¹H NMR spectrum (400 MHz) of complex 3 in DMSO-*d*₆ showing a sharp singlet for its diastereotopic methylene protons at room temperature (25°C), indicating DMSO is involved in the interconversion process.

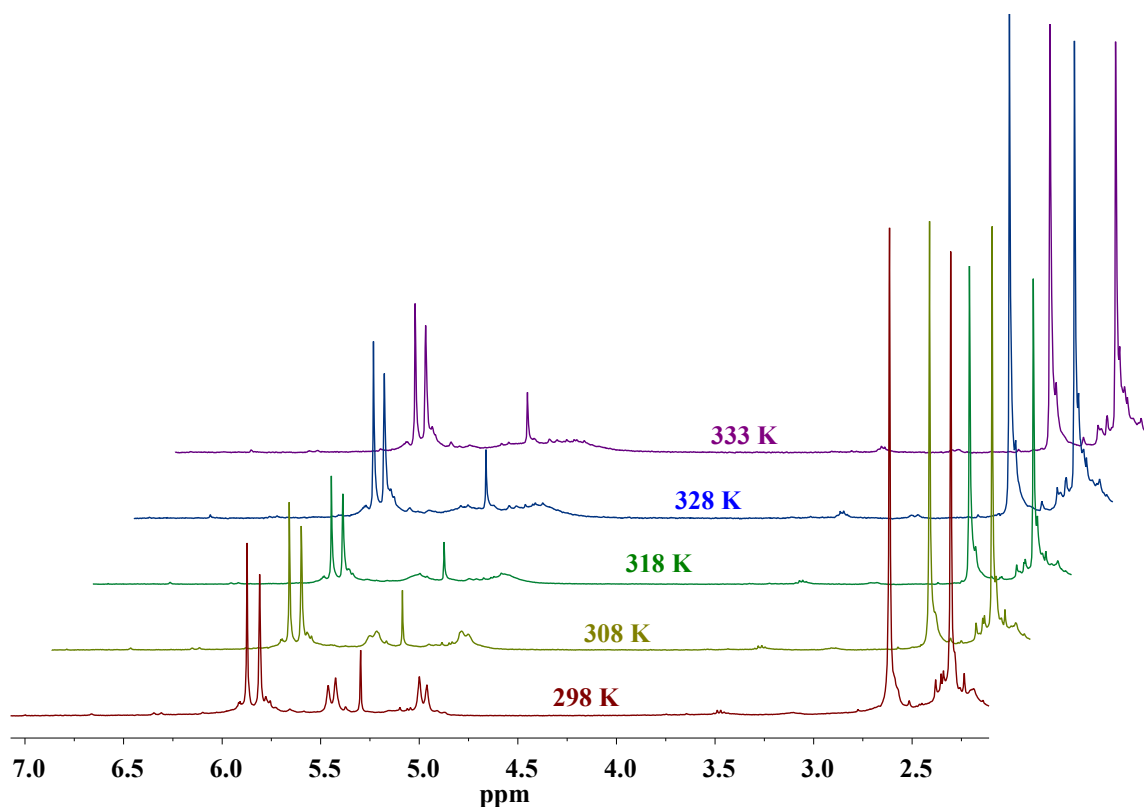


Figure S20. Variable-temperature ¹H-NMR spectra (400 MHz) of complex **5** in CDCl₃ (0.024 M) showing a broad singlet for its diastereotopic methylene protons at 60 °C due to the fast interconversion between the two enantiomers on the NMR time scale. The peak at 5.30 is due CH₂Cl₂.

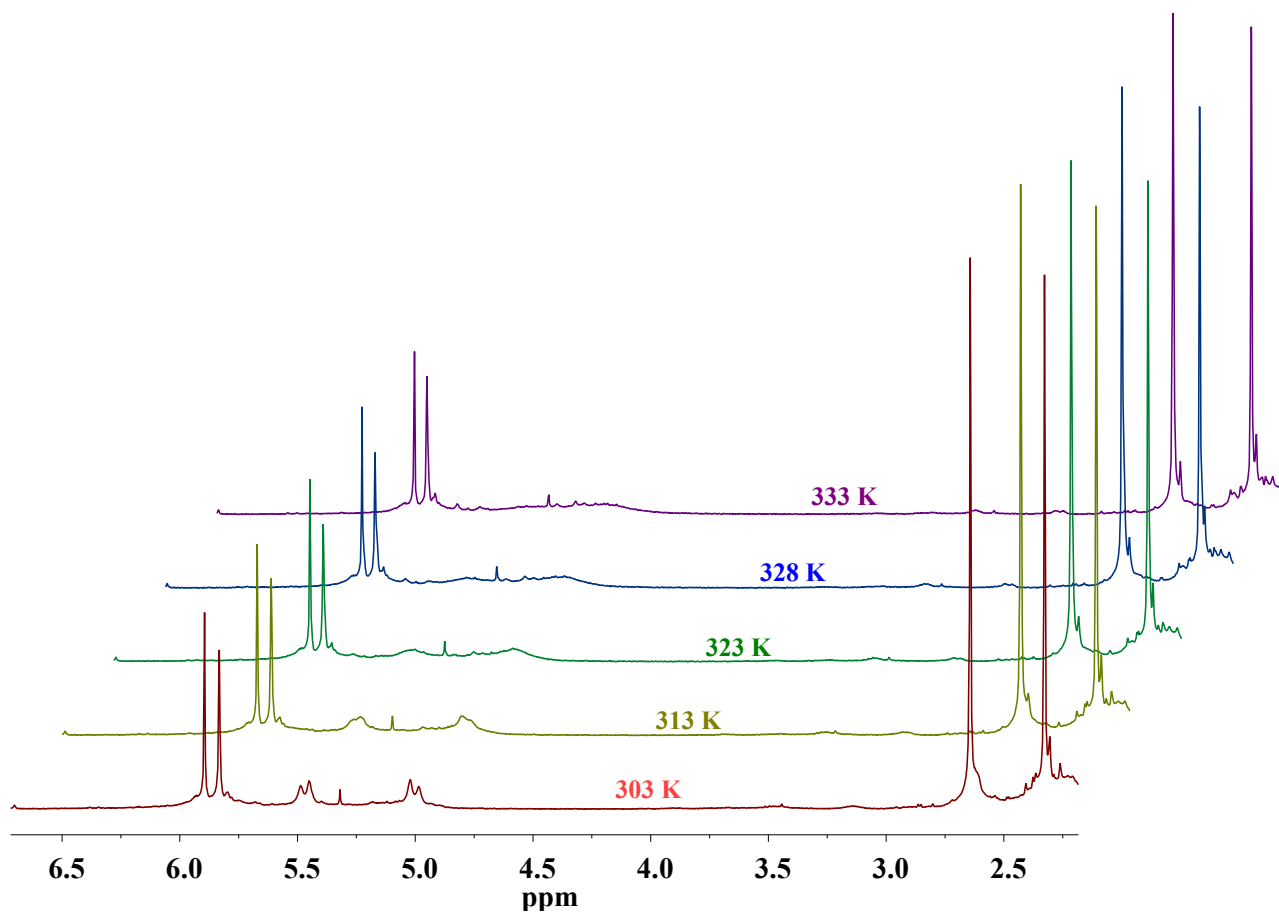


Figure S21. Variable-temperature ¹H-NMR spectra (400 MHz) of complex **5** in CDCl₃ (0.04 M) showing a broad singlet for its diastereotopic methylene protons at 60 °C due to the fast interconversion between the two enantiomers on the NMR time scale. The coalescence temperature *T*_c is the same as that observed for 0.024 M sample.

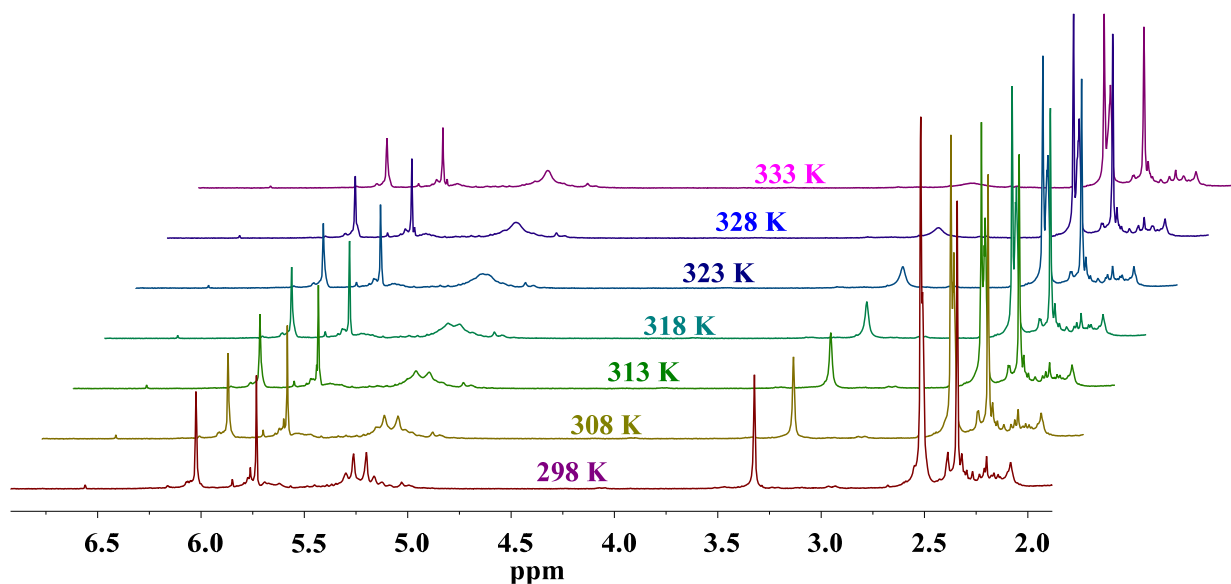


Figure S22. Variable-temperature ¹H-NMR spectra (400 MHz) of complex **5** in DMSO-*d*₆ (0.04 M), showing a broad singlet for its diastereotopic methylene protons at 50 °C due to the fast interconversion between the two enantiomers on the NMR time scale. DMSO is involved in the interconversion process.

II. X-ray Crystallography

Crystal structure of 2,5-bis(3,5-dimethylpyrazolylmethyl)pyrrole, **2**

The interesting feature of the structure of **2** is the *trans* or perpendicular orientation of the two pyrazole rings to the mean plane formed by the pyrrole ring and the two methylene carbon atoms, which minimizes the steric congestion between the pyrazole moieties.

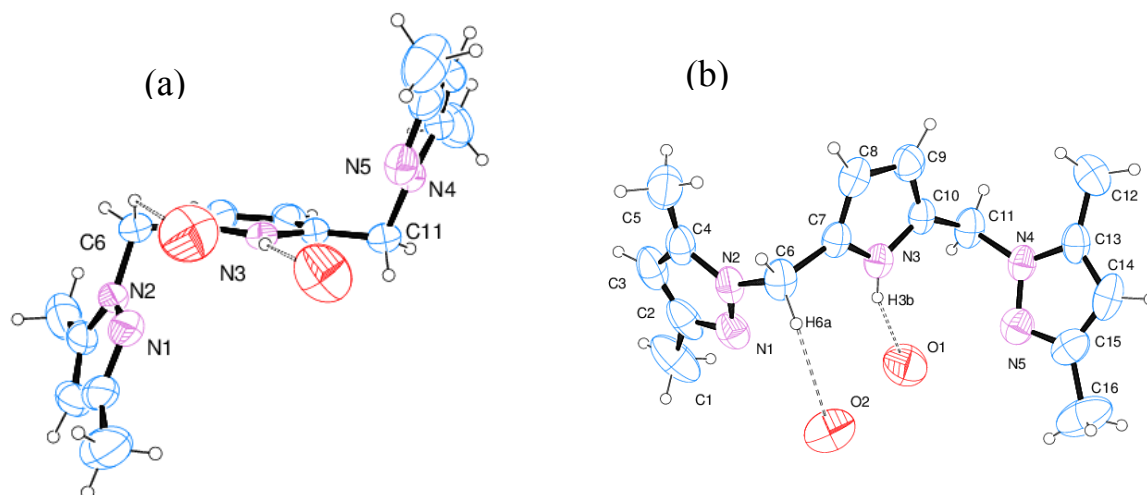


Figure S23. Molecular structure of **2**: (a) side view and (b) top view with 30% thermal ellipsoids.

The disordered oxygen atoms of the two water molecules are omitted. Dotted lines indicate hydrogen bonds. Selected bond lengths (Å) and angles (°): N1–N2 1.339(5), N2–C6 1.473(6), C6–C7 1.490(6), N3–C7 1.354(5), C7–C8 1.359(6), C8–C9 1.415(7), C9–C10 1.360(6), N3–C10 1.365(6), C10–C11 1.463(6), N4–C11 1.466(5), N4–N5 1.372(6), N1–N2–C6 121.0(5), C4–N2–N1 112.9(5), C7–N3–C10 111.7(4), C13–N4–N5 112.1(5), N5–N4–C11 117.9(5), N2–C6–C7 111.9(3), N3–C10–C11 122.7(6), C10–C11–N4 112.3(3).

Table S1 Crystallographic data for compounds **2·2H₂O**

	2·2H₂O
Empirical formula	C ₁₆ H ₂₅ N ₅ O ₂
Formula weight	319.41
Wavelength (Å)	0.71073
Temperature (K)	293(2)
Crystal system	Orthorhombic
Color and shape	Colorless, needle
Space group	<i>Pca2</i> ₁
<i>a</i> /Å	25.795(7)
<i>b</i> /Å	4.4057(12)
<i>c</i> /Å	16.118(4)
<i>α</i> /degree	90.00
<i>β</i> /degree	90.00
<i>γ</i> /degree	90.00
Volume(Å ³)	1831.7(9)
<i>Z</i>	4
<i>D</i> _{calcd} , g cm ⁻³	1.158
<i>μ</i> /mm ⁻¹	0.079
<i>F</i> (000)	688
Crystal size/mm	0.35×0.05×0.04
<i>θ</i> range(degree)	1.58 to 25.00
Limiting indices	-30≤ <i>h</i> ≤30 -5≤ <i>k</i> ≤5 -19≤ <i>l</i> ≤18
Total/ unique no. of reflns.	19760 / 3221
<i>R</i> _{int}	0.1100
Data / restr./ params.	3221 / 1 / 215
GOF(<i>F</i> ²)	1.005
<i>R</i> 1, <i>wR</i> 2	0.0553, 0.1147
<i>R</i> 1, <i>wR</i> 2 (all data)	0.1565, 0.1627
peak and hole (e Å ⁻³)	0.102 and -0.104

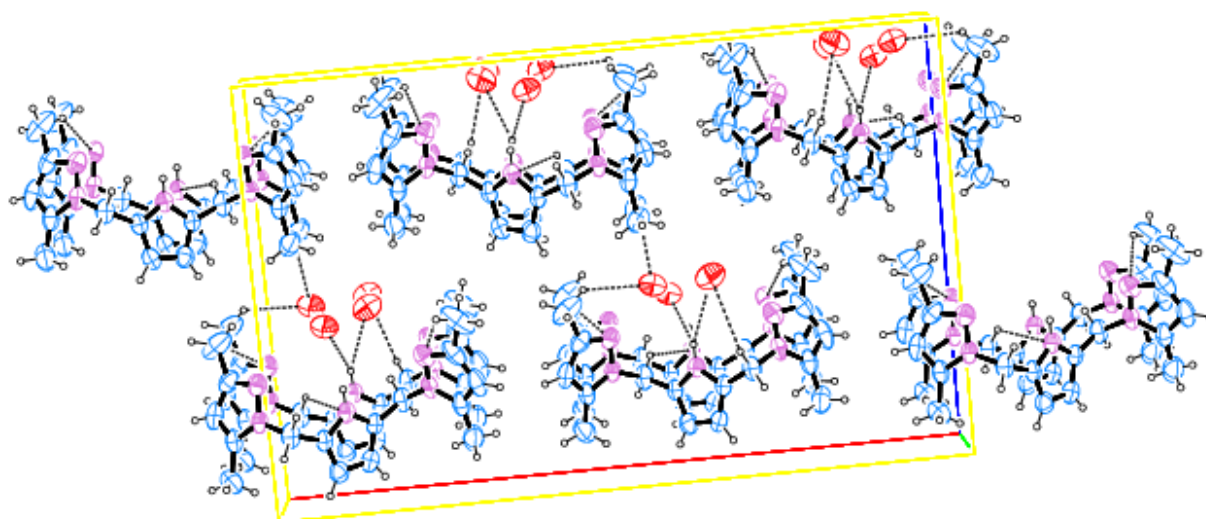


Figure S24. Unit cell packing diagram for $2 \cdot 2\text{H}_2\text{O}$.

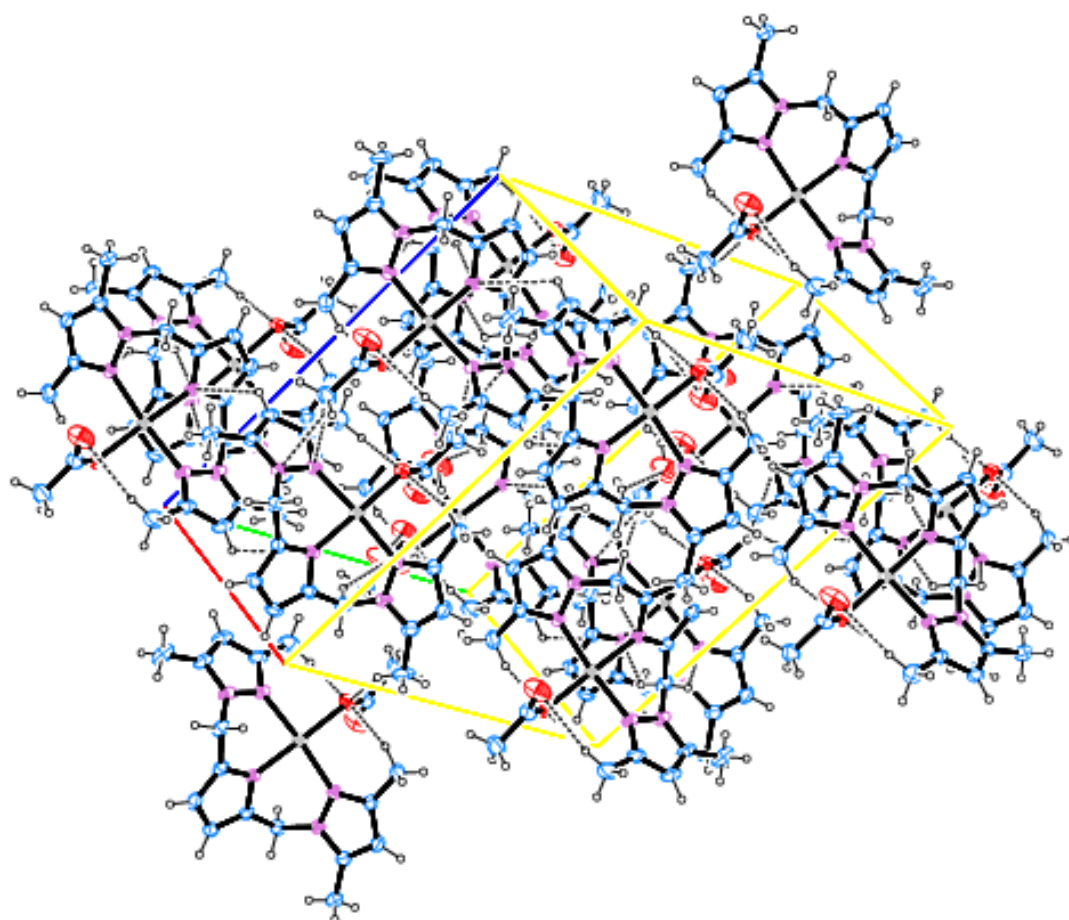


Figure S25. Unit cell packing diagram for $(3 \cdot \text{H}_2\text{O})_2$

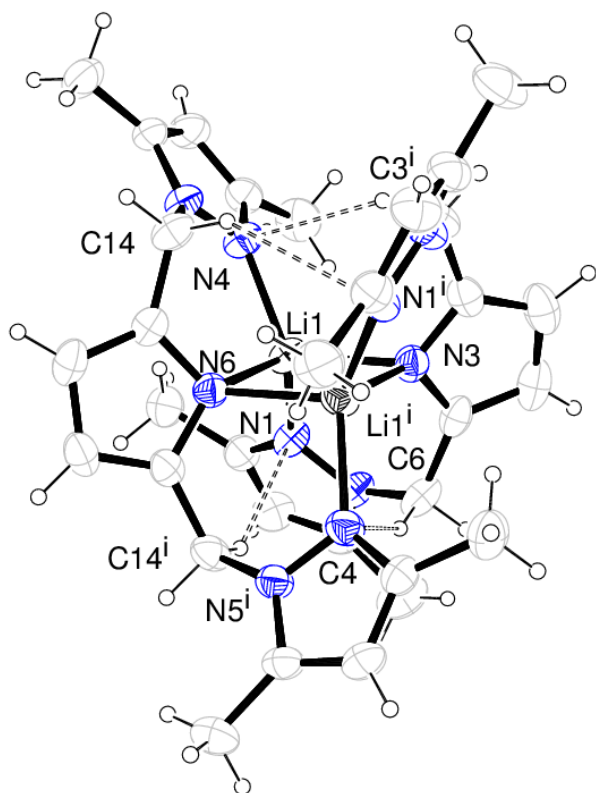


Figure S26. Molecular structure of the lithium salt of the pincer ligand, **4** (30% thermal ellipsoids).

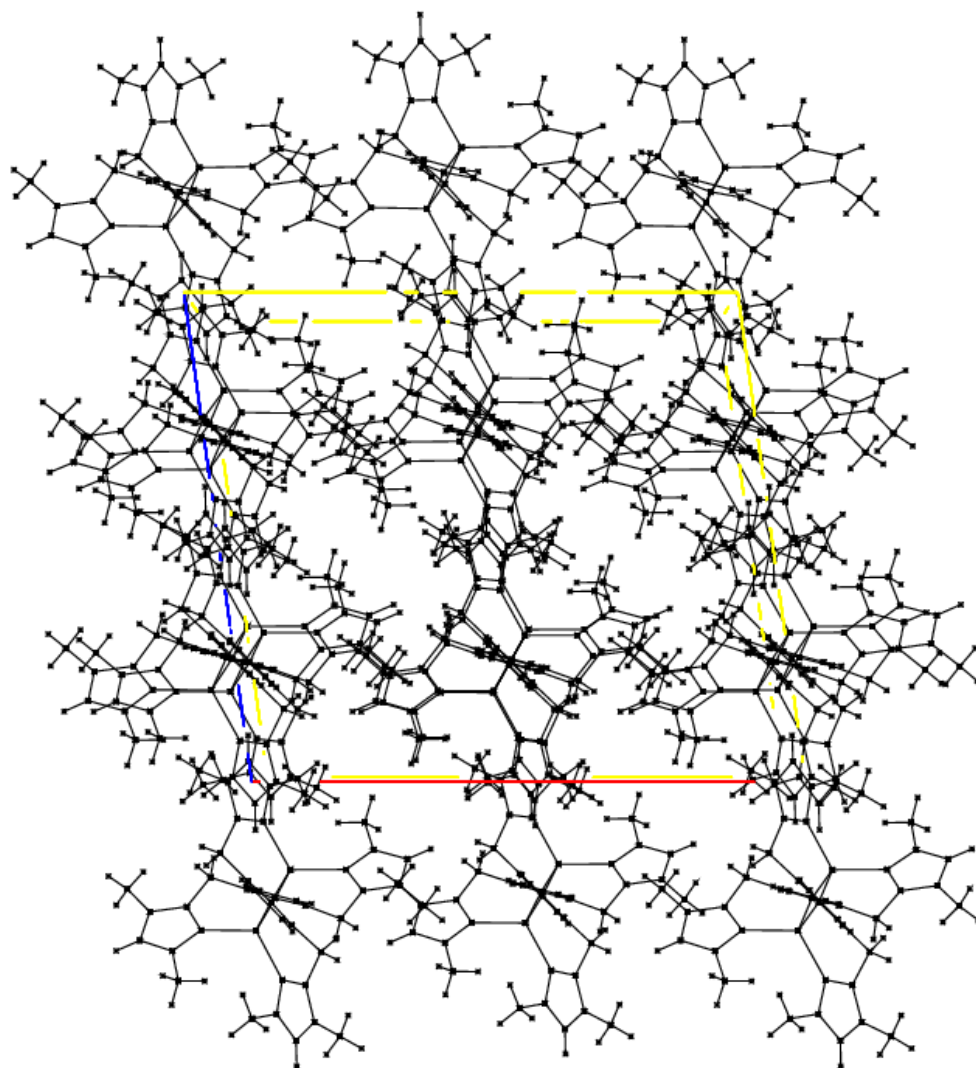


Figure S27. Unit cell packing diagram for **4**.

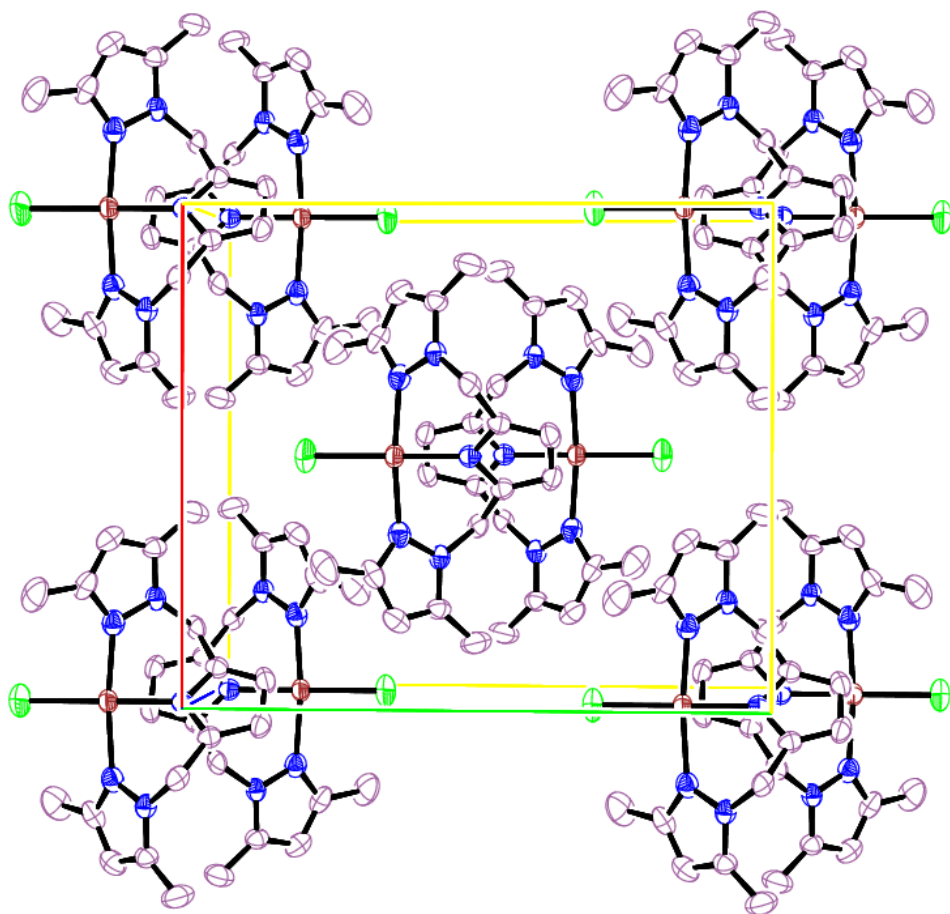


Figure S28. Unit cell packing diagram for **5**.

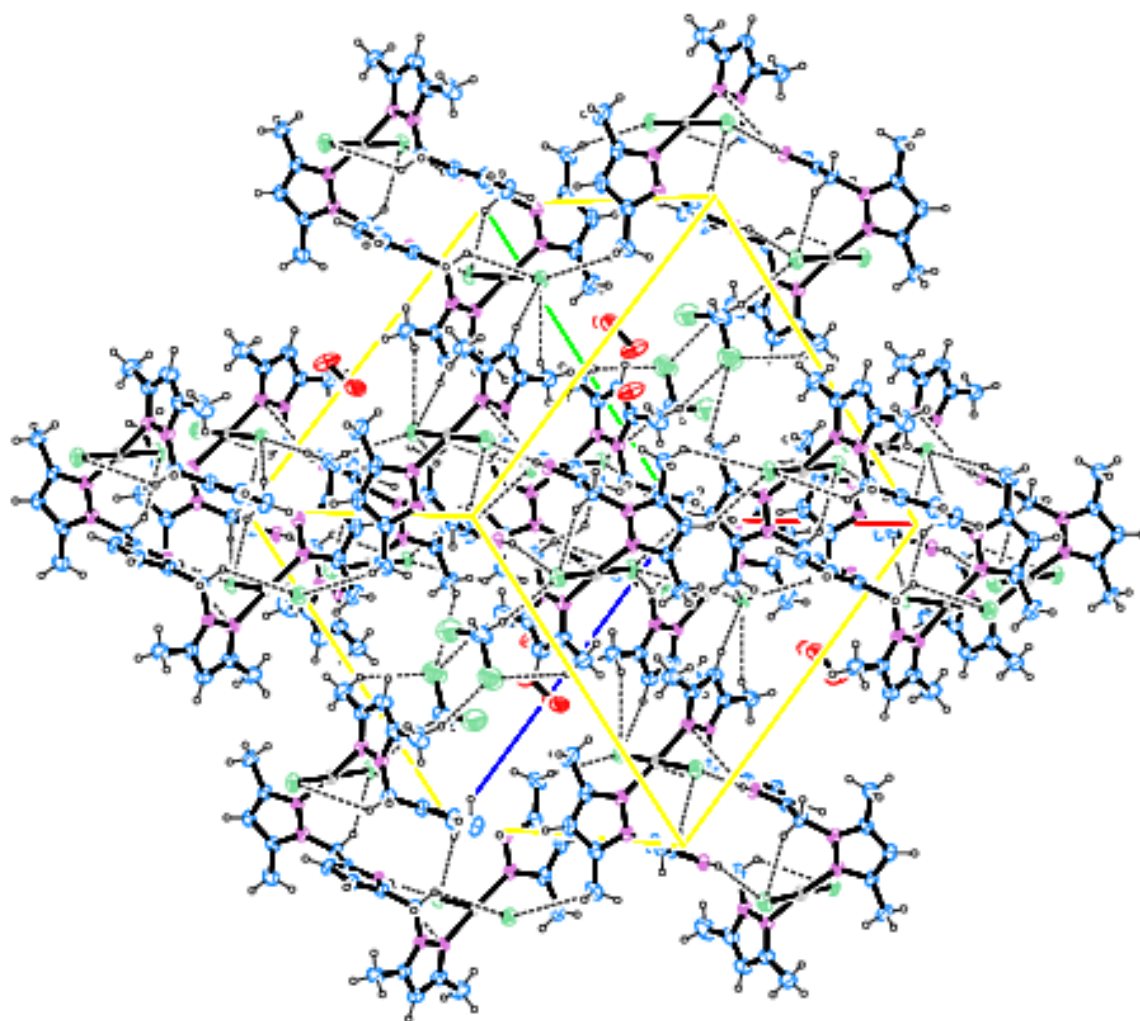


Figure S29. Unit cell packing diagram for $6 \cdot \text{CH}_2\text{Cl}_2 \cdot 2\text{H}_2\text{O}$.